Available online at www.sciencedirect.com

SciVerse ScienceDirect

journal homepage: www.elsevier.com/locate/he

A study on crystal structure, bonding and hydriding properties of Ti–Fe–Ni intermetallics – Behind substitution of iron by nickel

Katarina D. Ćirić [a,*], Andraž Kocjan [b,c], Anton Gradišek [b,d], Vasil J. Koteski [a], Ana M. Kalijadis [e], Valentin N. Ivanovski [a], Zoran V. Laušević [e], Dragica Lj. Stojić [f]

[a] Department of Nuclear and Plasma Physics, Vinča Institute of Nuclear Sciences, P.O. Box 522, University of Belgrade, 11000 Belgrade, Serbia
[b] "Jožef Stefan" Institute, Jamova cesta 39, SL-1000 Ljubljana, Slovenia
[c] NAMASTE Centre of Excellence, Jamova cesta 39, SI-1000 Ljubljana, Slovenia
[d] EN-FIST Centre of Excellence, Dunajska 156, SL-1000 Ljubljana, Slovenia
[e] Department of Physics, Vinča Institute of Nuclear Sciences, P.O. Box 522, University of Belgrade, 11000 Belgrade, Serbia
[f] Department of Physical Chemistry, Vinča Institute of Nuclear Sciences, P.O. Box 522, University of Belgrade, 11000 Belgrade, Serbia

ARTICLE INFO

Article history:
Received 14 December 2011
Received in revised form
30 January 2012
Accepted 9 February 2012
Available online 10 March 2012

Keywords:
Metal hydride
Ti–Fe–Ni
DFT
Hydrogen storage
Melt-spinning

ABSTRACT

Intermetallic compound TiFe, known for its hydrogen storage applications, is modified by substituting iron by nickel and related changes of properties and applicability of the obtained compounds are studied. Samples $TiFe_{1-x}Ni_x$ ($x = 0.2–0.6$) are synthesized by melt-spinning and their crystal structure, desorption characteristics and electronic structure are investigated by TPD, ^1H NMR and Mossbauer spectroscopy. State-of-the-art DFT calculations give further insight into the changes in electronic structure and bonding related to the hydrogen absorption and substitution of iron by nickel. The increase of Ni/Fe ratio in the $TiFe_{1-x}Ni_x$ is found to result in the increase of hydride cohesive energies and in the systematic shifting of Fermi energy (E_F) to lower values, in both pure intermetallics and appropriate hydrides. Hydride formation was found to influence the Fermi energy lowering and the increase of number of states at E_F.

1. Introduction

Metal hydrides, widely investigated class of materials, have possible applications in the hydrogen storage related problems, where reversibility and mild conditions of the hydrogen sorption process are required [1–3]. The AB-type alloys are promising materials for hydrogen absorption/desorption from the gas phase as well as for reversible electrochemical charging/discharging (metal hydride electrodes) [4–8]. The main representative of this class of materials is the intermetallic compound TiFe, which crystallizes in the cubic CsCl-type structure and can absorb reversibly up to 1.9 wt% hydrogen. The application of TiFe has been limited due to the poor absorption/desorption kinetics in addition to the complicated activation procedure and high equilibrium pressure for the hydride formation at room temperature [9]. Lots of experimental work has been done in order to improve the hydrogen storage properties of TiFe-type intermetallic compounds through substituting one of the two elements [8,10–15]. By substituting a part of the Fe atoms in TiFe with

* Corresponding author. Tel./fax: +381 11 2453681.
E-mail address: kciric@vinca.rs (K.D. Ćirić).
0360-3199/$ – see front matter
doi:10.1016/j.ijhydene.2012.02.047

metals like Mn, Ni, Cr, V, Ti, etc. the activation of the alloy is facilitated and the hydride equilibrium pressures is lowered. The polycrystalline Ti–Fe–Ni system has been widely studied in the past [16–19]. Also, it was reported that the respective replacement of Fe in TiFe by Ni and by Mn improved not only the discharge capacity but also the cycle life of the electrodes prepared from nanocrystalline TiFe alloys, synthesized by mechanical alloying and annealing [20]. The development of functional materials for application in energy sources and storage presents special challenges since they are required to satisfy multiple requirements [1]. In order to better understand the influence of the crystal structure and metal substitutions, state-of-the-art calculations are performed. Different DFT methods were employed in studying TiFe and TiNi hydrides [21–24]. Also, the influence of the replacement of Fe by different d-metals (Ni, Mn) on the bonding and electronic structure has been studied [25]. The band structure calculations were reported for pure Ti–Fe–Ni intermetallic compounds [20]. However, to the authors best knowledge, no investigation has been performed to examine the electronic structure and bonding in the hydrides with respect to the gradual nickel to iron substitution.

In this work, the hydriding properties of Ti–Fe–Ni intermetallics are systematically studied, by means of DFT calculations and experimental investigation, in order to gain knowledge about the quantitative relations between their composition and hydride phase properties. FP-LAPW band structure calculations reveal contribution of each atom to the electronic and bonding properties in Ti–Fe–Ni intermetallics and their hydrides.

2. Methods

2.1. Experimental

The precursors for the melt-spinning process were prepared by arc-melting the proper amounts of elemental Ti (99.9%), Fe (99.9%) and Ni (99.9%) powders pressed into pellets. These ingots were melted by induction heating in graphite crucibles. At 1673 K the melt was ejected onto a rotating copper cooling wheel with circumferential velocity 22 m/s. These brittle ribbons were pulverized in the mortar and subsequently annealed for 2 h at 973 K in dynamic vacuum (10^{-5} mbar) to obtain crystalline samples, which were subjected to activation at 573 K. The activated samples were subsequently hydrogenated at 10 bar and 50 bar for 8 h at 373 K in Sievert's apparatus. The crystal structure before and after hydrogenation was determined with a Bruker AXS, D4 Endeavor diffractometer using Cu-Ka radiation. Hydrogen desorption experiments were performed by Carbolite electric furnace at heating rate 20 K/min and the final temperature 973 K. Samples were placed in a silica tube, which was attached to Edwards turbo vacuum pump that yielded 10^{-5} mbar vacuum. Hydrogen content was determined upon pressure change dependence on the temperature. The Mössbauer absorption spectrum was obtained in a standard transmission geometry with the constant acceleration using a source ^{57}Co in Rh (1.85 GBq) at room temperature. The sample was embedded in aluminum foils with the surface density of 10.0 mg/cm^2. In order to calibrate the Mössbauer spectrum, the laser spectrum of velocity was recorded. Both spectra were obtained in 1024 channels and folded in the same manner. The Mössbauer data and the laser data were analyzed by WinNormos-Site program [27]. Isomer shifts were calculated with respect to α-Fe. The ^{1}H Nuclear Magnetic Resonant spectroscopy (NMR) measurements were conducted using a 100 MHz Oxford superconducting magnet ($B = 2.35$ T). ^{1}H spin-lattice relaxation time, T_1, was measured as a function of temperature in the temperature range from 80 K to 420 K.

2.2. Calculations method

Substitution of iron by nickel in TiFe intermetallic compound preserves the original CsCl-type structure (B2 structure, Pm3m space group) [28]. It is known that upon hydrogenation of TiFe several phases emerge, depending on the amount of the absorbed hydrogen: cubic, α phase, for small amounts of hydrogen; orthorhombic, β phase, $TiFeH_y$ ($y = 1.4$) and monoclinic, γ phase ($y = 2$) [23]. In all of these phases as well as in TiNiH [29], hydrogen occupies octahedral interstices. As a first approach to the calculation of the electronic structure and bonding properties of Ti–Fe–Ni hydrides, the calculations were done assuming CsCl-type structure of hydrides (this is experimentally determined structure of α phase hydrides).

In order to model the substitution of iron by nickel in the crystal cell, supercells $TiFe_{0.75}Ni_{0.25}$, $TiFe_{0.5}Ni_{0.5}$ and $TiFe_{0.25}Ni_{0.75}$ were constructed out of eight formula units of TiFe, and the appropriate hydrides were obtained by placing hydrogen atom in the octahedral sites, as shown in Fig. 1. Taking into account the efficiency of the calculation, compromise of half occupancy of the octahedral Ti_4M_2 sites (M = Fe, Ni) by hydrogen in all cases was adopted giving hydrogen to metal ratio, H/M, 0.75. Since in $TiFe_{0.75}Ni_{0.25}$ and $TiFe_{0.25}Ni_{0.75}$ supercells used in our calculations, not all octahedral sites are equivalent as they are in TiFe, the above condition of the half occupancy of Ti_4M_2 octahedral sites leads to different coordination around the hydrogen atom. This is schematically given at Fig. 1, where (a) and (b) are the labels adopted for this hydrides and they are used further throughout the text. The electronic band structure calculations were performed for the supercells representing the pure Ti–Fe–Ni intermetallic compounds (Fig. 1), appropriate hydrides (both (a) and (b) if present) as well as for TiNi and TiFe. All calculations have been done using the full-potential linearized augmented plane wave (FP-LAPW) method based on the density functional theory (DFT), as implemented in the WIEN2k code [30]. For the exchange–correlation potential generalized gradient approximation (GGA) of Perdew et al. was used [31]. The potential and charge density were expanded up to $l = 10$ and $G_{max} = 16$ (20) bohr^{-1} for pure intermetallics (and hydrides). The muffin-tin radii were set to 0.8 bohr for H, 1.9 bohr for Ti and 1.8 bohr for both Ni and Fe atoms. The RK_{max} cut-off parameter was set to 5.0 for the hydrides and 10.0 for the pure intermetallics, giving roughly the same number of the plane waves in the calculations and ensuring the accuracy of calculation. Reciprocal space integrations were performed using the tetrahedron method on 250 and 560 irreducible k-points ($20 \times 20 \times 20$ and $28 \times 28 \times 28$ k-point meshes), for the supercells and TiFe (TiNi), respectively. The

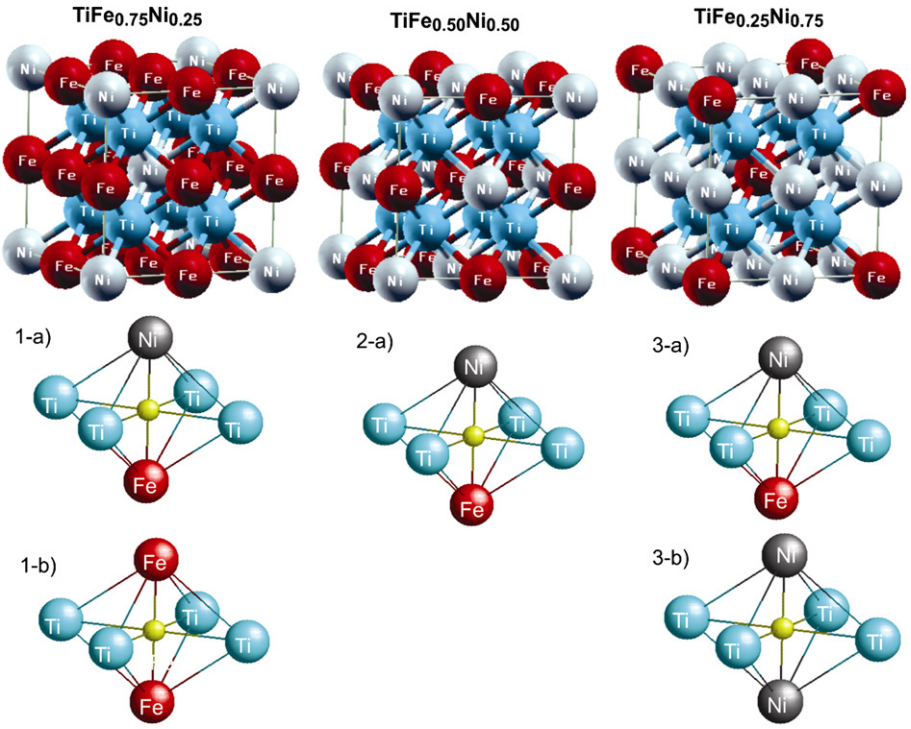

Fig. 1 – Supercells $TiFe_{0.75}Ni_{0.25}$, $TiFe_{0.5}Ni_{0.5}$, $TiFe_{0.25}Ni_{0.75}$ constructed out of eight formula units of TiFe; the appropriate hydrides are obtained by putting hydrogen atoms (two smallest balls) in octahedral sites, as presented in picture, 1–3. Marks -a and -b present different coordination around hydrogen as explained in text. The picture was obtained using XCrysDen program [26].

experimental results for TiFe lattice parameters and atomic positions [32] were used as starting parameters, and then, volume optimization and internal parameters relaxation (until the forces acting on the atoms were smaller than 1 mRy/bohr) were performed for each compound. From the Birch–Murnaghan equation of state the ground state energy and optimized structural parameters were extracted. The charge difference of $5*10^{-5}e$ between the two successive iterations was chosen as the convergence criterion. The core states were treated fully relativistically, while the valence states were treated within the scalar relativistic approximation. Additional spin-polarized calculation was performed for TiFe, but no significant difference was found as compared to the non-spin polarized case; this is also in accordance with earlier investigations [21]. Therefore, all the remaining calculations were performed non-spin polarized.

3. Results and discussion

3.1. *Crystal structure of $TiFe_{1-x}Ni_x$ (x = 0.2, 0.4, 0.6)*

The XRD spectra for the melt-spun ribbons of $TiFe_{1-x}Ni_x$ ($x = 0.2, 0.4, 0.6$), given at Fig. 2, show single bcc phase for all compositions, which is in agreement with the results exhibited in Ref. [28] for alloys obtained by arc-melting.

The $TiFe_{1-x}Ni_x$ alloys (iron-site substituted alloys) have a CsCl-type structure, which is the same structure as that of the starting material, TiFe [28]. On the other hand, the $Ti_{1-x}FeNi_x$ alloys (titanium-site substituted alloys) are a mixture of CsCl-type and a C14 Laves phase compound [28]. Our XRD results are consistent with structure of CsCl-type for all investigated samples. Also, the increase of the lattice constant upon the increase of nickel content is observed, and this trend is in agreement with the results obtained from our DFT calculations given in Table 1. In addition, Mössbauer spectrometry is also a method that gives very precise structural information on materials, with reference to the iron atom. In Section 3.4 is confirmed, on the basis of the obtained Mössbauer spectra, that applied method of sample preparation resulted in total iron-site substitution.

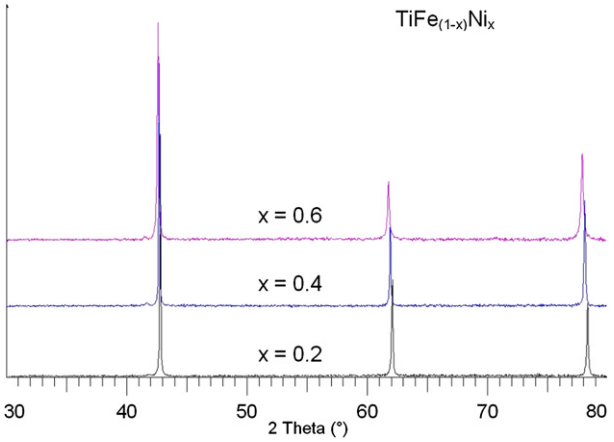

Fig. 2 – XRD spectra of $TiFe_{1-x}Ni_x$ melt-spun ribbons.

Table 1 – Optimized structural parameters, bulk moduli, B, Fermi level characteristics and cohesive energies from DFT calculations of $TiFe_{1-x}Ni_x$.

	a (Å)		B (GPa)	E_F (Ry[a])	N_{EF}	E_c (eV/atom)
	calc.	exp.				
TiFe	2.955	2.979[b]	188.55	0.904	0.421	6.41
$TiFe_{0.75}Ni_{0.25}$	2.973		184.29	0.87492	1.331	6.35
$TiFe_{0.5}Ni_{0.5}$	2.984		174.51	0.85131	2.315	6.32
$TiFe_{0.25}Ni_{0.75}$	3.004	3.01[b]	170.57	0.82015	2.482	6.29
TiNi	3.010	3.018[b]	158.19	0.73950	2.756	5.89

a 1Ry = 13.6 eV.
b M. Jurczyk et al. [33].

3.2. *Hydrogen sorption characteristics of $TiFe_{1-x}Ni_x$ (x = 0.2, 0.4, 0.6) by TPD analysis*

The substitution of iron by nickel was reported to lower the equilibrium pressure for hydrogen absorption [14] and improve the kinetics of this process [19]. Here, the influence of this substitution in TiFe on desorption characteristics of the appropriate hydrides was investigated using Temperature Programmed Desorption (TPD), after previously loading the samples in hydrogen atmosphere at 10 and 50 bars.

In Fig. 3 TPD spectra for $TiFe_{1-x}Ni_x$ after loading at 50 bar hydrogen for 8 h are presented. The increase of Ni content lowers the maximal hydrogen absorption capacity at those conditions, from 1.1 wt%H for x = 0.2, to 0.8 wt%H for x = 0.4 and 0.1 wt%H for x = 0.6. Further conclusion from TPD spectrum is that the increase of Ni content increases the desorption temperature. This is also true when hydrogen is loaded at lower pressure (10 bar), but in that case desorption temperatures are found to be systematically shifted to lower values. The thermal stability of the hydrides is in agreement with hydrides enthalpy of formation, i.e. it increases with increased nickel content, as reported earlier in Ref. [14].

3.3. *DFT investigation of the electronic structure and bonding in $TiFe_{1-x}Ni_x$ intermetallics and the appropriate hydrides*

The optimized structural parameters obtained from the band structure calculations on $TiFe_{1-x}Ni_x$ intermetallics (x = 0, 0.25, 0.5, 0.75, 1), are presented in Table 1. They are found to be in good agreement with the available experimental results. In Table 2, the results obtained for the appropriate hydrides are presented.

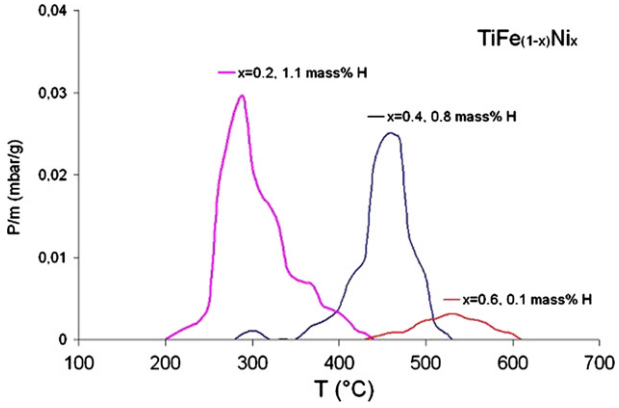

Fig. 3 – TPD results of hydrogenated (373 K, 50 bar, 8 h) $TiFe_{1-x}Ni_x$ (x = 0.2, 0.4, 0.6) samples.

Results for hydrides, with hydrogen atom occupying both non-equivalent hydrogen sites in investigated hydrides, are presented and in the further discussion labeled according to Fig. 1. The lattice constants of hydrides are larger than that of the pure intermetallics and dependent on the Ni/Fe ratio (or starting lattice constant). This increase of lattice constant is in accordance with the volume increase, typical for interstitial hydrides. The bulk moduli, which are a measure of the metal hardness, decrease upon both alloying with Ni and hydrogen absorption. Decrease of the bulk moduli of hydrides as compared to the starting intermetallics implies that some of the metal–metal bonds are significantly weakened upon hydrogen absorption. Calculated cohesive energies for hydrides show increase with increase of Ni/Fe ratio in intermetallic. The larger cohesive energy relates to the stronger bonds between the elements. As can be seen by comparing results for hydrides (Table 2) with results for pure intermetallics (Table 1), observed trend is characteristic only for hydrides and implies stronger bonded hydrogen in the host lattice. This explains the lowering of equilibrium pressure for hydrogen absorption [14] and here observed desorption temperature increase with increase of Ni/Fe ratio. More detailed analysis of bonding in hydrides based on density of states (DOS) and Bader analysis is given below. The analysis of electronic structure in hydrogen-free intermetallic compounds can be found, and our results on these compounds are in good agreement with those obtained by Szajek et al. [20]. Total density of states for $TiFe_{1-x}Ni_x$ (x = 0.25, 0.50, 0.75) alloys and the appropriate hydrides is presented in Fig. 4, with the Fermi energy (E_F) taken as reference.

In all cases, with and without hydrogen, the alloys exhibit metallic character (finite DOS at the Fermi energy). Similarly to other metallic hydrides, hydrogen presence induces significant changes in the valence band of intermetallic compounds, mostly by introduction of new states located 6 eV–11 eV below the Fermi energy. By examining the results presented in Table 1, we observe systematic shifting of Fermi energy (E_F) to lower values, whereas number of states at E_F (N_{EF}) increases upon nickel addition in the intermetallic compounds. All hydrides (Table 2.) have lower values of E_F as compared to the starting compounds, regardless of the

Table 2 – Optimized structural parameters, bulk moduli, B, Fermi level characteristics and cohesive energies from DFT calculations of the appropriate hydrides of $TiFe_{1-x}Ni_x$ (x = 0.25,0.5,0.75) with non-equivalent hydrogen sites (a, b).

	a (Å)	B (GPa)	E_F (Ry[a])	N_{EF}	E_c (eV/atom)
$TiFe_{0.75}Ni_{0.25}H_{1.5}$-a	3.139	175.36	0.814	4.237	4.553
$TiFe_{0.75}Ni_{0.25}H_{1.5}$-b	3.145	165.14	0.797	4.132	4.555
$TiFe_{0.5}Ni_{0.5}H_{1.5}$	3.141	169.07	0.794	2.653	4.575
$TiFe_{0.25}Ni_{0.75}H_{1.5}$-a	3.161	167.10	0.761	3.482	4.577
$TiFe_{0.25}Ni_{0.75}H_{1.5}$-b	3.155	158.43	0.770	2.301	4.596

a 1Ry = 13.6 eV.

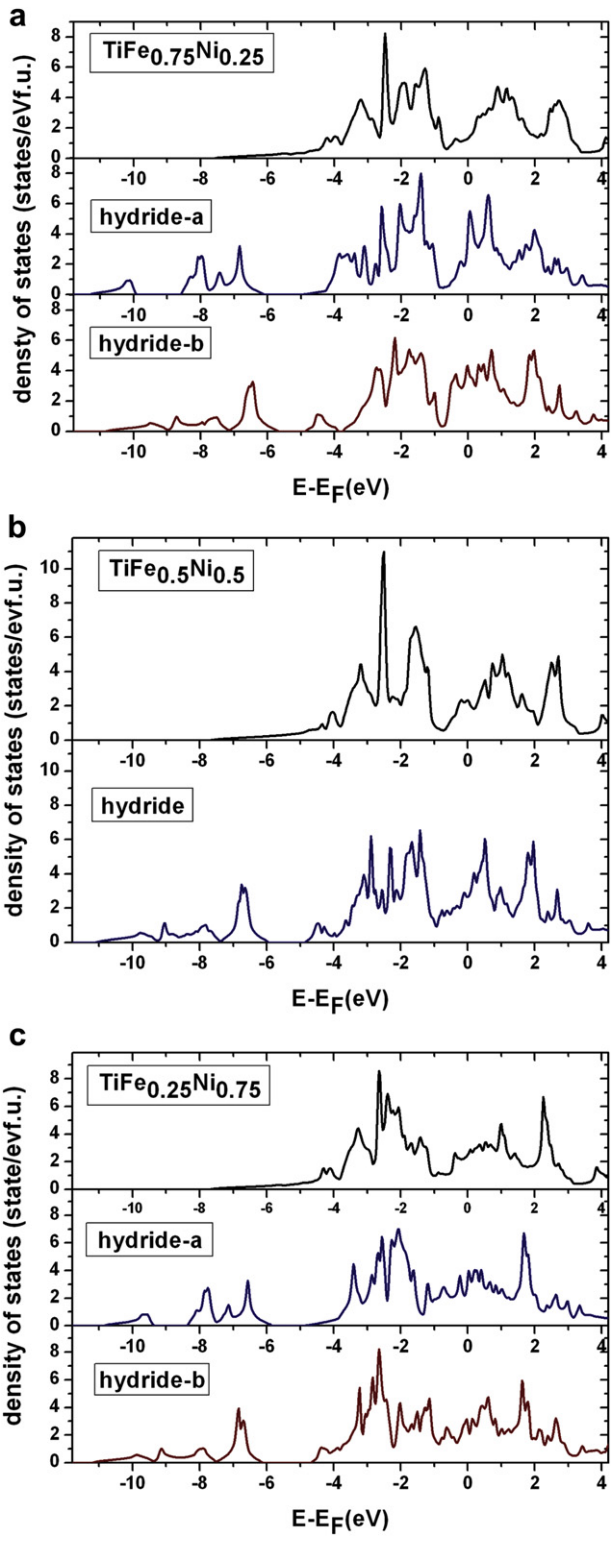

Fig. 4 – Total density of states of Ti–Fe–Ni intermetallics and their hydrides (a) $TiFe_{0.75}Ni_{0.25}$ (b) $TiFe_{0.5}Ni_{0.5}$ (c) $TiFe_{0.25}Ni_{0.75}$ (for $x = 0.25, 0.75$ hydride labels according to Fig. 1).

position of hydrogen in the octahedral sites. The general trend of lower E_F in intermetallics with higher Ni/Fe ratio is preserved in the hydrides, too. However, the hydrides show largest N_{EF} in $TiFe_{0.75}Ni_{0.25}$, which decreases with nickel addition. The Figs. 5–8 present the partial density of states of Ni, Fe, Ti and H, per atom. For $TiFe_{0.25}Ni_{0.75}$ and $TiFe_{0.75}Ni_{0.25}$, the DOS shown is an arithmetic mean of the DOS for different calculated hydrogen coordinations.

As expected, the Ti, Ni and Fe valence bands are determined by their d states, while for H, the most dominant is the s channel. The contribution of Ti-d states is mainly at energies higher than E_F, Fig. 5. This trend is retained upon hydride formation, with appearance of some Ti states in the region 6 eV–11 eV. The Ni-d states are located mainly below E_F, before and after hydrogenation (Fig. 7). Both iron and nickel density of states show appearance of new states in the hydrides, located at the energies of hydrogen s states (Fig. 8a), so we can conclude that all metals, Ti, Fe and Ni interact with hydrogen and that hydride formation is dominated by interaction of metal d states and hydrogen s state. In the hydrides, due to the changes induced by hydrogen, number of states is much larger at E_F than in starting intermetallics. In TiFe, the Fermi energy falls into the semi-gap of iron d states, which explains the relatively low number of states at E_F. This is somewhat changed when iron is substituted by nickel, Table 1. In the hydrides, semi-gap of the iron d-states is at the energies below E_F, explaining the larger number of states at E_F. This is most pronounced in the case of $TiFe_{0.75}Ni_{0.25}$ hydride, whose average DOS in proximity of E_F is presented at Fig. 8b. Here, the largest contribution to E_F DOS comes from titanium and iron d states, and this is also case in other hydrides, explaining observed N_F decrease with iron to nickel substitution. The topological analyses of the electron densities following Bader's atoms-in-molecules (AIM) theory [34] was used to characterize the bonding situation and quantify effect of the hydrogenation in Ti–Fe–Ni intermetallics. This method gives a partitioning of the crystal space into atomic basins. By integration within these basins atomic (AIM-) charges are obtained, and they show the amount of charge in atomic basin in some compound as compared to the neutral atom [34]. The integrated charges for Ti–Fe–Ni, prior to hydrogen absorption, show charge transfer in the accordance with elements electronegativity. Both Ni and Fe atoms have more negative charge as compared to neutral atoms (more negative AIM-charge), and the sum of this excess charge on these atoms (taking into account their abundance in the unit cell) equals the charge that Ti atom have lost. The larger the amount of nickel in the intermetallics, the more positive AIM-charge is found at Ti atoms, while both Fe and Ni have smaller negative AIM-charge. The charge transfer trend is the same in the case of the appropriate hydrides, but now excess charge is divided among Fe, Ni and H.

This is schematically given in Fig. 9, for the pure intermetallics and their hydrides (average value of transferred charge is presented for hydrides which have two possible coordinations around hydrogen in calculations). In the hydrides, Ti loses even more charge as compared to the pure intermetallics, and Ni still shows larger negative AIM-charge as compared to Fe. But what is very interesting is the fact that in all hydrides the hydrogen atom AIM-charge is the same within the error of the calculation (−0.45). Similar value is found in some other hydrides [35]. The charge transferred to hydrogen in metal hydrides varies from the values close to 1, in what is referred to as ionic hydrides (magnesium hydride), to values

below 0.5, mostly in intermetallic hydrides [35]. Here obtained value of 0.45 indicates more covalent character of the hydrogen–metal interaction. Also, if less charge is transferred to the hydrogen atom, the appropriate hydride is expected to be less stable [36]. In our case, although the charge transfer between atoms should be affected by the replacement of iron with more electronegative nickel atoms, the charge transferred to hydrogen atom seems to be almost invariant of this composition change. Additional calculations would have to be done

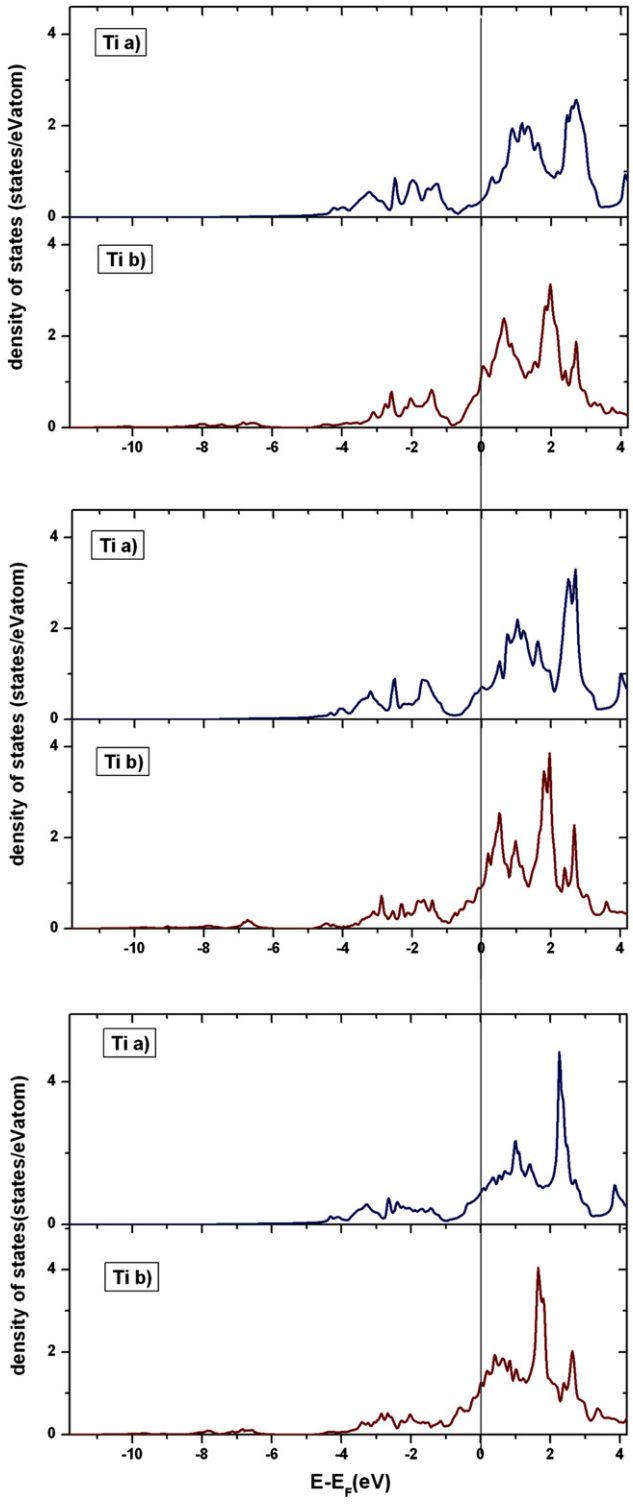

Fig. 5 – Partial (d-projected) DOS for Ti; going from top to bottom $TiFe_{0.75}Ni_{0.25}$, $TiFe_{0.5}Ni_{0.5}$ and $TiFe_{0.25}Ni_{0.75}$ are presented, where (a) presents intermetallic compound and (b) appropriate hydride.

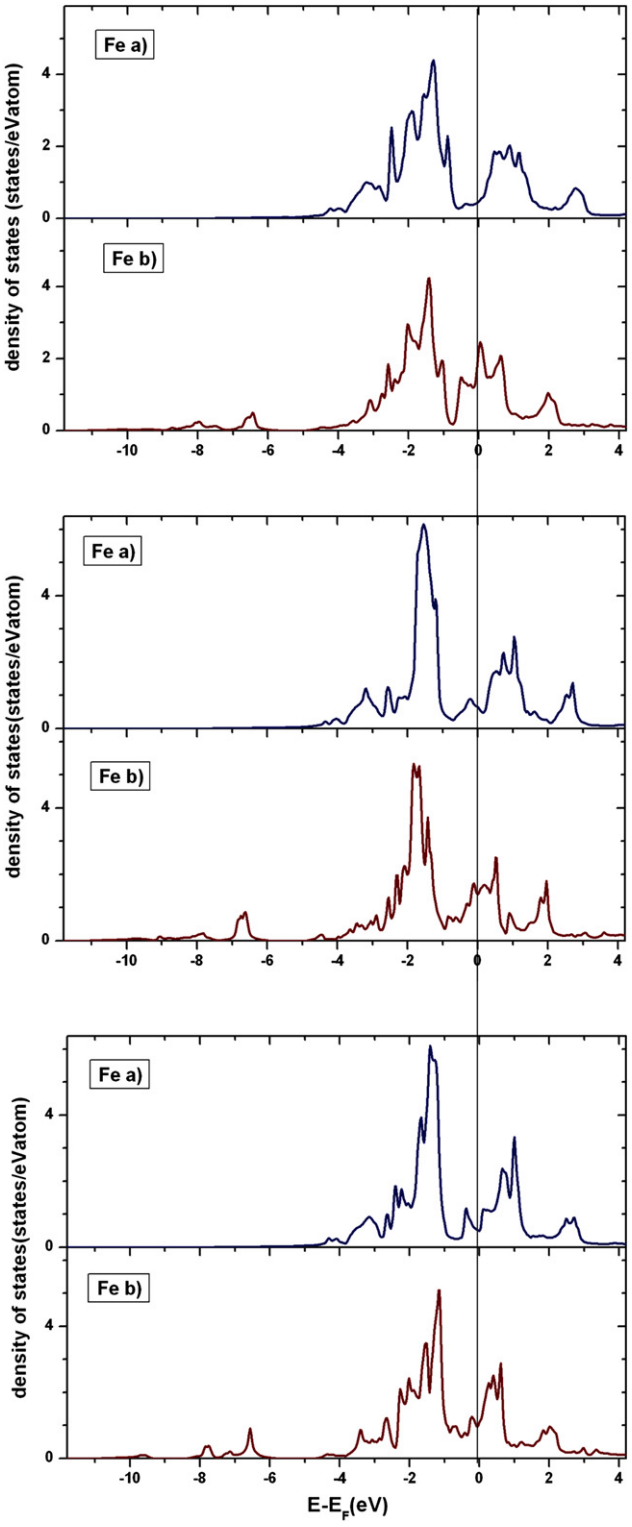

Fig. 6 – Partial (d-projected) DOS for Fe; Going from top to bottom $TiFe_{0.75}Ni_{0.25}$, $TiFe_{0.5}Ni_{0.5}$ and $TiFe_{0.25}Ni_{0.75}$ are presented, where (a) presents intermetallic compound and (b) appropriate hydride.

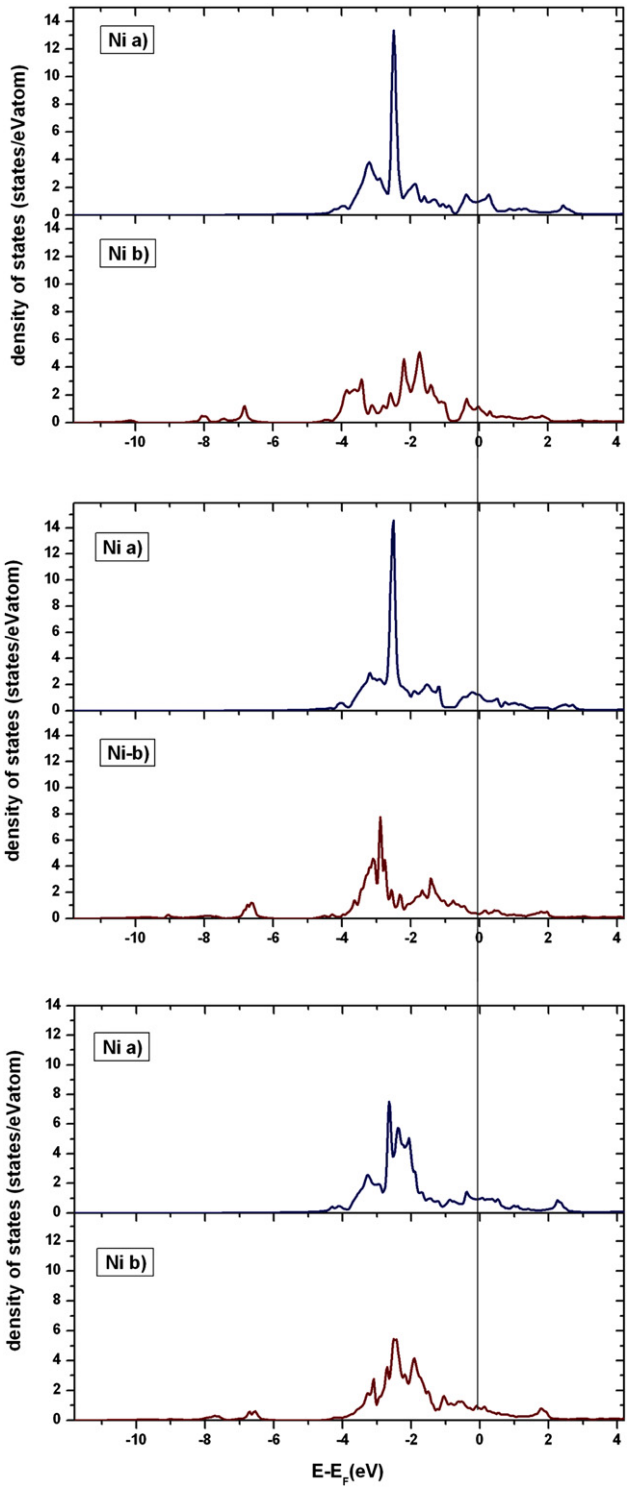

Fig. 7 – Partial (d-projected) DOS for Ni; Going from top to bottom $TiFe_{0.75}Ni_{0.25}$, $TiFe_{0.5}Ni_{0.5}$ and $TiFe_{0.25}Ni_{0.75}$ are presented, where (a) presents intermetallic compound and (b) appropriate hydride.

in order to see the influence of structural changes in hydrides on the charge transfer. However, some experimental methods offer the possibility of investigation of electronic structure, and this is discussed in next chapter.

3.4. *Mössbauer and NMR investigation of hydrides*

Mössbauer spectroscopy has been used to study both lattice structure changes and changes in the electronic structure upon hydrogen absorption in $TiFe_{1-x}Ni_x$ intermetallics. The Mössbauer spectra (^{57}Fe) were recorded for pure intermetallics as well as after hydriding at 10 bar hydrogen pressure for 20 h. For all investigated samples, before hydrogenation, the Mössbauer spectra were fitted with one doublet. Small quadrupole splitting is observed in accordance with the change in the first coordination sphere of iron upon nickel substitution. The presence of only one doublet in fitted spectra is a very sensitive indicator of presence of just one phase in these samples, which, along with the XRD results, confirm total iron-site substitution. In Fig. 10 the Mossbauer spectra of $TiFe_{0.6}Ni_{0.4}$ before and after hydrogenation are presented.

Before hydrogenation (Fig. 10a), the doublet is characterized with isomer shift (IS) $\delta = -0.155(1)$ mm/s and the quadrupole splitting $\Delta = 0.138(4)$ mm/s. Upon hydrogen absorption, the spectrum has two components (Fig. 10b) and this is related to the presence of two phases in the sample [36]. The first phase is characterized with isomer shift (IS): $\delta = -0.162(2)$ mm/s and quadrupole splitting $\Delta = 0.115(4)$ identified based on Ref. [36] as cubic solid solution (alpha phase); the isomer shift in this phase is very close to that of starting intermetallic. This would indicate that the iron atom in alpha phase had no changes in electron density that would affect IS. From Bader analysis we saw that the small charge transfer to hydrogen is expected in hydrides, even in the case of a high hydrogen concentration in the intermetallic lattice. Since in experiment, lower concentrations of hydrogen are expected in alpha phase, and just a part of that charge originates from iron atom, this can be an explanation of the small change in isomer shift. More detailed analysis of Mössbauer spectra in all compounds will be published elsewhere. The second phase identified ($\delta = -0.105(8)$, $\Delta = 0.45(1)$) is orthorhombic hydride phase (beta phase) [36]. Thus, we can conclude that the obtained Mössbauer spectrum indicates a coexistence of alpha and beta phase, where, based on integrated surfaces under picks, their relative amounts are estimated to be 80 and 20%, respectively. We see that the process of beta hydride formation is related to the decrease of negative isomer shift and increase of quadrupole splitting. The smaller negative isomer shift is due to the smaller electron density in the absorber (iron atom). This change of the isomer shift upon hydrogen absorption can be understood in the way that upon forming of Fe–H bond, more charge is transferred to hydrogen and this was also observed in other intermetallic hydrides [37,38]. Increase of quadrupole splitting in the beta phase hydride compared to both, the starting intermetallic and alpha phase hydride, is related to the symmetry decrease around Fe atom that follows the phase change.

NMR measurements were performed on a series of Ti–Fe–Ni samples with different amounts of hydrogen absorbed. For protons in a metallic system, there are two major relaxation mechanisms – relaxation through fluctuations in dipolar interaction between protons; and by the proton coupling to the spin of magnetic moments of the conducting electrons in the metal. While both mechanisms contribute to the relaxation at higher temperatures, the proton movement slows down at lower temperatures, thus enabling us to extract

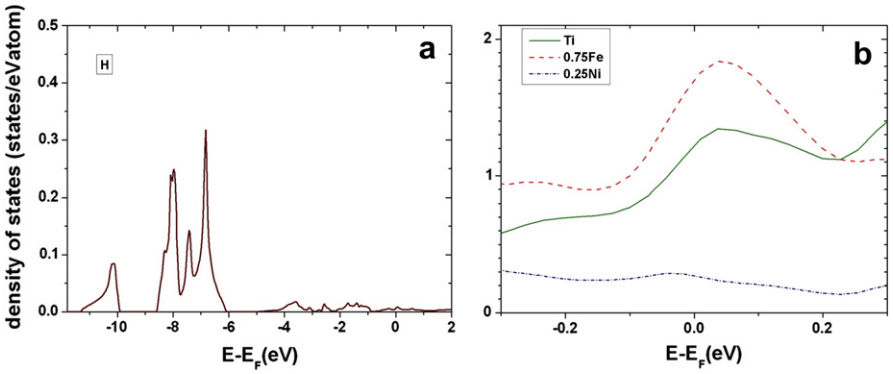

Fig. 8 – (a) Partial (site-projected) density of states of hydrogen atom (b) partial (d-projected) density of states of Ti, Fe and Ni near Fermi energy in $TiFe_{0.75}Ni_{0.25}$ hydride.

the electron contribution. Relaxation through conducting electrons follows the Korringa relation, $1/(T_1T) = C \times \rho(E_F)^2$, where constant C includes the proton and electron gyromagnetic ratios and the Knight shift [39]. Although the structure slightly changes upon loading with hydrogen, it should in principle be possible to compare the measured values at different loading levels with the theoretical calculations. Similar work was performed for example in Ref. [40], where the ^{1}H NMR measurements demonstrated that there is no significant difference between the electronic structures in a series of Ti–Zr–Ni alloys with slightly different compositions.

Fig. 11 shows ^{1}H spin-lattice relaxation rate, T_1^{-1}, as a function of inverse temperature for the crystalline $TiFe_{0.75}Ni_{0.25}$ sample with three different hydrogen concentrations. All three concentrations show similar behavior. At higher temperatures, there is a peak in relaxation, connected to the dipolar relaxation mechanism. However, at lower temperatures, the relaxation is not proportional to the temperature as one would expect from the above model, but rather approaches a constant value. Further on, the proton relaxation rates at low temperatures are significantly faster than in previously investigated systems of the Ti–Zr–Ni family, where T_1^{-1} at 80 K was around 0.5 s^{-1} [40].

The reason for this behavior is an additional relaxation mechanism, most likely connected with relaxation through paramagnetic centers (Fe and Ni) in the system. In a metallic crystal, the magnetic moments of atoms are shielded by the electron gas. Due to defects in the material, induced by introducing hydrogen, the local density of electron states changes and the shielding becomes less prominent, resulting in a higher magnetic moment [41]. As a first approximation, it is reasonable to assume that this contribution to relaxation is temperature independent [42]. As this mechanism masks the contribution of the conducting electrons, it is not possible to obtain the information about the electronic density at the Fermi level from the NMR measurements. The paramagnetic contribution appears to be larger for samples with 0.84 wt% and 1.03 wt%, what seems to be consistent with the fact that the larger concentration of introduced hydrogen creates more defects in the material.

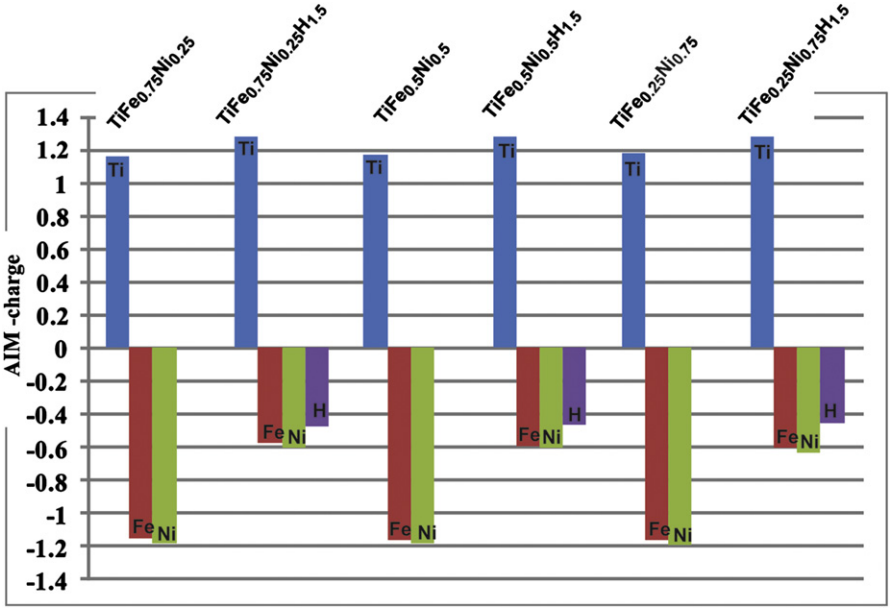

Fig. 9 – Calculated AIM-charges in Ti–Fe–Ni intermetallics and their hydrides.

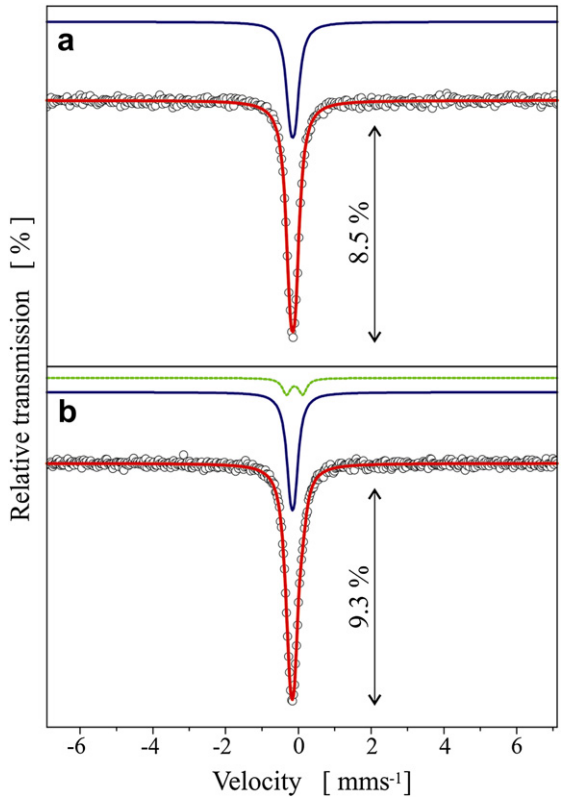

Fig. 10 – Mossbauer spectrum of $TiFe_{0.6}Ni_{0.4}$ before hydriding consists of one narrow doublet subspectrum – the first line from the top of figure (a); after hydriding spectrum contains two doublet subspectra given by lines on the top of figure – the upper one corresponds to beta phase hydride and the lower one to alpha hydride (b); experimental data (presented by open circles) and fitted spectrum (solid line) are given on the bottom of both figures.

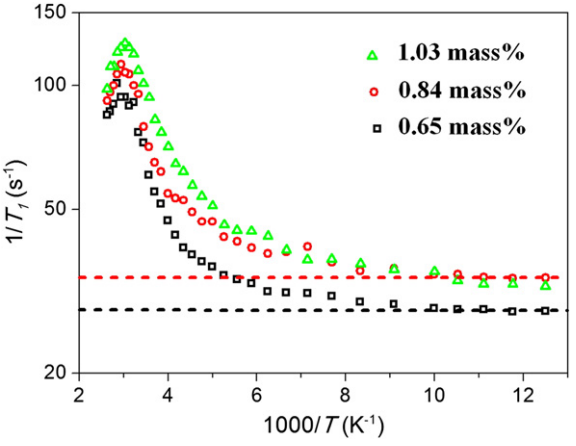

Fig. 11 – Spin-lattice relaxation rate, T_1^{-1}, as a function of inverse temperature for $TiFe_{0.75}Ni_{0.25}$ sample with three different hydrogen loading levels. Dashed lines serve as guide to an eye, indicating the paramagnetic contribution to the relaxation.

4. Conclusion

Crystalline samples $TiFe_{1-x}Ni_x$, obtained by melt-spinning, were all found to have bcc structure implying that, in all ratios investigated (0.2–0.6), solubility of nickel in the TiFe lattice was complete. The stability of $TiFe_{1-x}Ni_x$ hydrides was investigated by TPD, and it was found that the increase of nickel content leads to the shifting of hydrogen desorption temperatures to higher values and decrease of maximal amounts of hydrogen absorbed at the same conditions (hydrogen pressure, time). The values of the cohesive energies calculated for hydrides increase as the Ni/Fe ratio in the appropriate intermetallic compound increases, which explains observed influence of nickel addition to the hydrogen sorption equilibrium pressure lowering. Based on the above stated, $TiFe_{0.8}Ni_{0.2}$ is found to be most promising among here studied materials for the hydrogen storage. Investigating changes that follow hydrogen insertion in the intermetallic lattices on atomic level we report detailed analysis of the electronic structure and bonding in investigated compounds, which can be useful in future investigation of metal hydrides for application in Ni-MH batteries; main conclusions are summarized below. The increase of Ni/Fe ratio in intermetallic compound leads to systematic shifting of Fermi energy (E_F) to lower values, both before and after hydriding. The hydrogen–metal bond formation is dominantly due to the interaction of metal d states and hydrogen s state located 6–11 eV below Fermi energy, and all metals participate in this. Hydride formation was found to influence the Fermi energy lowering and the increase of number of states at E_F (as compared to the starting intermetallics); the latter is mostly related to the changes in Fe and Ti-d states. Due to the new-formed metal–hydrogen bonds, charge transferred between metal atoms is smaller than in the pure intermetallics, as confirmed by Bader charge analysis. Interestingly, the charge transfer to hydrogen atom in calculated structures was found to be almost the same (0.45*e*) regardless of Fe/Ni ratio in intermetallic lattice. However, from Mössbauer spectra we can conclude that upon structural changes in crystal lattice (namely beta hydride formation) charge transfer from iron atom to hydrogen atom further increases. From NMR investigation it was not possible to obtain the information about the electronic density at the Fermi level, which was explained as consequence of hydrogen induced defect in the lattice. Beside dipolar relaxation mechanism, additional relaxation mechanism, most likely connected with relaxation through paramagnetic centers in the system, is found. Results are consistent with the fact that the larger concentration of introduced hydrogen creates more defects in the examined material.

Acknowledgment

The Ministry of Science and Technological Development of the Republic of Serbia provided the financial support for this study through the Project No. 171 001. The authors also thank Dr Tomaž Apih for help with measurements and discussion related to NMR.

REFERENCES

[1] Sakintuna B, Lamari-Darkrim F, Hirscher M. Metal hydride materials for solid hydrogen storage. A review. Int J Hydrogen Energy 2007;32:1121–40.

[2] Liu Y, Pan H, Gao M, Wang Q. Advanced hydrogen storage alloys for Ni/MH rechargeable batteries. J Mater Chem 2011; 21:4743–55.

[3] Eberle U, Arnold G, von Helmolt R. Hydrogen storage in metal–hydrogen systems and their derivatives. J Power Sources 2006;154(2):456–60.

[4] Zhao X, Ma L. Recent progress in hydrogen storage alloys for nickel/metal hydride secondary batteries. Int J Hydrogen Energy 2009;34:4788–96.

[5] Bououdina M, Grant D, Walker G. Review on hydrogen absorbing materials-structure, microstructure, and thermodynamic properties. Int J Hydrogen Energy 2006;31: 177–82.

[6] Buschow KHJ, Bouten PCP, Miedema AR. Hydrides formed from intermetallic compounds of two transition metals: a special class of ternary alloys. Rep Prog Phys 1982;45: 937–1039.

[7] Kleperis J, Wójcik G, Czerwinski A, Skowronski J, Kopczyk M, Beltowska-Brzezinska M. Electrochemical behavior of metal hydrides. J SolidState Electrochem 2001;5(4):229–49.

[8] Abrashev B, Spassov T, Bliznakov S, Popov A. Microstructure and electrochemical hydriding/dehydriding properties of ball-milled TiFe-based alloys. Int J Hydrogen Energy 2010;35: 6332–7.

[9] Reilly JJ, Wiswall RH. Formation and properties of iron titanium hydride. Inorg Chem 1974;13(1):218–22.

[10] Singh BK, Singh AK, Srivastava ON. On the synthesis, characterization and hydrogenation behaviour of $Fe_{1-x}Ti_{1+y}Ni_x$ ($x = 0.2$, $y = 0.3$) hydrogen storage material. Int J Hydrogen Energy 1997;22(8):805–8.

[11] Lee SM, Perng T-P, Juang HK, Chen SY, Chen WY, Hsu SE. Microstructures and hydrogenation properties of $TiFe_{1-x}M_x$ alloys. J Alloys Compd 1992;187:49–57.

[12] Lee SM, Perng T-P. Effect of the second phase on the initiation of hydrogenation of Ti–$Fe_{1-x}M_x$ (M = Cr, Mn) alloys. Int J Hydrogen Energy 1994;19:259–63.

[13] Boulghallat M, Gerard N. Hydriding kinetics of $TiFe_{0.5}Co_{0.5}$ compounds. J Less-Common Met 1991;172–174:1052–7.

[14] Lee SM, Perng T-P. Correlation of substitutional solid solution with hydrogenation properties of $TiFe_{1-x}M_x$ (M = Ni, Co, Al) alloys. J Alloys Compd 1999;291:254–61.

[15] Wang CS, Lei YQ, Wang QD. Effects of Nb and Pd on the electrochemical properties of a Ti–Ni hydrogen-storage electrode. J Power Sources 1998;70:222–7.

[16] Jurczyk M. Nanocrystalline metal hydride electrode materials. Curr Top Electrochem 2003;9:105–16.

[17] Jurczyk M, Jankowska E, Makowiecka M, Wieczorek I. Electrode characteristics of nanocrystalline TiFe-type alloys. J Alloys Compd 2003;354:L1–4.

[18] Mintz MH, Vaknin S, Biderman S, Hadari Z. Hydrides of ternary $TiFe_xM_{1-x}$ (M=Cr, Mn, Co, Ni) intermetallics. J Appl Phys 1981;52:463–7.

[19] Bououdina M, Fruchart D, Jacquet S, Pontonnier L, Soubeyroux JL. Effect of nickel alloying by using ball milling on the hydrogen absorption properties of TiFe. Int J Hydrogen Energy 1999;24(9):885–90.

[20] Szajek A, Jurczyk M, Jankowska E. The electronic and electrochemical properties of the TiFe-based alloys. J Alloys Compd 2003;348:285–92.

[21] Kinaci A, Aydinol MK. Ab initio investigation of FeTi–H system. Int J Hydrogen Energy 2007;32:2466–74.

[22] Nambu T, Ezaki H, Yukawa H, Morinaga M. Electronic structure and hydriding property of titanium compounds with CsCl-type structure. J Alloys Compd 1999;293–295: 213–6.

[23] Gupta M, Rodriguez E. Recent investigations of the electronic structure of hydrides of intermetallic compounds. J Alloys Compd 1995;219(1–2):6–9.

[24] Liu HJ, Ye Y. Electronic structure and stability of Ti-based shape memory alloys by LMTO-ASA. Solid State Commun 1998;106(4):197–202.

[25] Yukawa H, Matsumura T, Morinaga M. Chemical bond state and hydride stability of hydrogen storage alloys. J Alloys Compd 1999;293–295:227–30.

[26] Kokalj A. XCrySDen – a new program for displaying crystalline structures and electron densities. J Mol Graphics Model 1999;17(3–4):176–9.

[27] Brand RA. Improving the validity of hyperfine field distributions from magnetic alloys part I: unpolarized source. Nucl Instr Methods Phys Res 1987;B28(3): 398–416.

[28] Miyamura H, Takada M, Hirose K, Kikuchi S. Metal hydride electrodes using titanium–iron-based alloys. J Alloys Compd 2003;356–357:755–8.

[29] Schmidt R, Schlereth M, Wipf H, Assmus W, Mullner M. Hydrogen solubility and diffusion in the shape-memory alloy NiTi. J Phys Condens Matter 1989;1(14):2473–82.

[30] Blaha P, Schwarz K, Sorantin P, Trickey SB. Full-potential, linearized augmented plane wave programs for crystalline systems. Comput Phys Commun 1990;59:399–415.

[31] Perdew JP, Burke K, Ernzerhof M. Generalized gradient approximation made simple. Phys Rev Lett 1996;77: 3865–8.

[32] Melnyk G, Tremel W. The titanium–iron–antimony ternary system and the crystal and electronic structure of the interstitial compound Ti_5FeSb_2. J Alloys Compd 2003; 349(1–2):164–71.

[33] Jurczyk M, Jankowska E, Nowak M, Jakubowic J. Nanocrystalline titanium-type metal hydride electrodes prepared by mechanical alloying. J Alloys Compd 2002; 336(1–2):265–9.

[34] Bader RFW. Atoms in molecules – a quantum theory. Oxford: Oxford University Press; 1990.

[35] Matar SF. Intermetallic hydrides: a review with ab initio aspects. Prog Solid State Chem 2010;38(1–4):1–37.

[36] Tetsuro A, Tanaka K, Shimotomai M, Doyama M. Structure and stability of hydrided FeNiTi compounds studied by X-ray diffraction and Mössbauer spectroscopy. Trans Jpn Inst Metals 1987;28:861–8.

[37] Aubertin F, Combell SJ, Gonser V. Hydrogenation of Zr_2Ni. Hyperfine Interact 1986;28:997–1000.

[38] Singh M, Jain IP. Mössbauer and positron life-time studies of FeTi and $Fe_{46}Ti_{50}Mn_4$ hydride systems. Int J Hydrogen Energy 1996;21:367–72.

[39] Slichter C. Principles of magnetic resonance. 3rd. Berlin: Springer; 1996. p. 156.

[40] Kocjan A, Kovačič S, Gradišek A, Kovač J, McGuiness PJ, Apih T, et al. Selective hydrogenation of Ti–Zr–Ni alloys. Int J Hydrogen Energy 2011;36(4):3056–61.

[41] Jagličić Z, Jagodič M, Grushko B, Zijlstra ES, Weber Th, Steurer W, et al. The effect of thermal treatment on the magnetic state and cluster-related disorder of icosahedral Al–Pd–Mn quasicrystals. Intermetallics 2010; 18:623–32.

[42] Phua T-T, Beaudry BJ, Peterson DT, Torgeson DR, Barnes RG, Belhoul M, et al. Paramagnetic impurity effects in NMR determinations of hydrogen diffusion and electronic structure in metal hydrides. Gd^{3+} in YH_2 and $LaH_{2.25}$. Phys Rev 1983;B28(11):6227–50.